small methods
www.small-methods.com

Rational Control of Near-Infrared Colloidal Thick-Shell Eco-Friendly Quantum Dots for Solar Energy Conversion

Lei Jin, Jiabin Liu, Xin Liu, Daniele Benetti, Gurpreet Singh Selopal, Xin Tong, Ehsan Hamzehpoor, Faying Li, Dmytro F. Perepichka, Zhiming M. Wang,* and Federico Rosei**

Thick-shell colloidal quantum dots (QDs) are promising building blocks for solar technologies due to their size/composition/shape-tunable properties. However, most well-performed thick-shell QDs suffer from frequent use of toxic metal elements including Pb and Cd, and inadequate light absorption in the visible and near-infrared (NIR) region due to the wide bandgap of the shell. In this work, eco-friendly $AgInSe_2/AgInS_2$ core/shell QDs, which are optically active in the NIR region and are suitable candidates to fabricate devices for solar energy conversion, are developed. Direct synthesis suffers from simultaneously controlling the reactivity of multiple precursors, instead, a template-assisted cation exchange method is used. By modulating the monolayer growth of template QDs, gradient AgInSeS shell layers are incorporated into $AgInSe_2/AgInS_2$ QDs. The resulting $AgInSe_2/AgInSeS/AgInS_2$ exhibits better charge transfer than $AgInSe_2/AgInS_2$ due to their favorable electronic band alignment, as predicted by first-principle calculations and confirmed by transient fluorescence spectroscopy. The photoelectrochemical cells fabricated with $AgInSe_2/AgInSeS/AgInS_2$ QDs present ≈1.5-fold higher current density and better stability compared to $AgInSe_2/AgInS_2$. The findings define a promising approach toward multinary QDs and pave the way for engineering the QDs' electronic band structures for solar-energy conversion.

1. Introduction

Among various renewable energy resources, solar radiation is particularly promising due to its relative abundance, sustainability, carbon neutrality, and cost-effectiveness.[1] Various semiconductors have been developed for converting solar energy into useful forms including electricity and clean chemical fuels.[2] Among them, colloidal quantum dots (QDs) are promising due to their size/composition/shape tunable optical and electronic properties arising from quantum confinement,[3] ease of fabrication through wet chemistry approaches, abundant surface binding sites, and the possibility of multiple exciton generation (MEG).[4] Recent years have witnessed a major improvement in QD-based solar energy technologies,[5] including solar cells,[6] luminescent solar concentrators (LSCs),[7] and photocatalysis.[8] However, one of the bottlenecks that hinder the performance of QD-based technologies is their sensitivity to their

L. Jin, X. Tong, Z. M. Wang
Institute of Fundamental and Frontier Sciences
University of Electronic Science and Technology of China
Chengdu 610054, P. R. China
E-mail: zhmwang@uestc.edu.cn

L. Jin, J. Liu, X. Liu, D. Benetti, F. Li, F. Rosei
Centre for Energy
Materials and Telecommunications
Institut national de la recherche scientifique
1650 Boul. Lionel-Boulet, Varennes, Quebec J3X 1P7, Canada
E-mail: rosei@emt.inrs.ca

L. Jin, D. Benetti, E. Hamzehpoor, D. F. Perepichka
Department of Chemistry
McGill University
801 Sherbrooke Street West, Montreal, Quebec H3A 0B8, Canada
E-mail: dmytro.perepichka@mcgill.ca

G. S. Selopal
Department of Engineering
Faculty of Agriculture
Dalhousie University
Truro, NS, B2N 5E3, Canada

Z. M. Wang
Institute for Advanced Study
Chengdu University
Chengdu, Sichuan 610106, P. R. China

The ORCID identification number(s) for the author(s) of this article can be found under https://doi.org/10.1002/smtd.202300133

DOI: 10.1002/smtd.202300133

surface environment (such as moisture, oxygen, temperature, and light) due to their large surface-to-volume ratio.[9] The dangling bonds of surface atoms can act as charge recombination centers, compromising the chemical/photostability and overall device performance.[9] An effective solution is to use a wide-bandgap semiconductor as a thick shell (>1.5 nm) to isolate the core from its surroundings and reduce possible surface traps.[10] In addition, the energy band structure of thick-shell QDs can be adjusted by appropriately choosing the core/shell materials,[10a,11] tuning the core-to-shell ratio and regulating the interfacial layers.[10e,12] Various thick-shell QDs have been developed for solar energy conversion, including CdSe/CdS and PbS/CdS for photoelectrochemical (PEC) solar-H_2 conversion,[10e,13] and CdSe/$CdSe_xS_{1-x}$/CdS QDs for solar cells.[14] Nevertheless, the presence of hazardous metal contents (e.g., Pb, and Cd) severely restrict their commercial-scale development. Alternatively, ternary I-III-VI QDs, including $AgInSe_2$ (AISe) have shown promise for solar energy conversion,[15] due to their high absorption coefficients in the visible wavelength region,[16] broadly tunable light absorption range (bulk bandgap of ≈1.19 eV)[17] and a structural tolerance to large stoichiometry off-sets. However, the existing shell for ternary QDs is only limited to wide-bandgap materials (e.g., 2.49 eV for CdS, 2.82 eV for ZnSe, and 3.54 eV for ZnS[18]). Due to the relatively large shell-to-core volume ratio, the absorption spectrum of thick-shell QDs is often dominated by the shell. Therefore, the wide bandgap of the shell results in insufficient visible and near-infrared light absorption of QDs. Theoretically, $AgInS_2$ (AIS) may serve as a suitable shell for AISe due to its suitable bandgap ≈1.87 eV and similar lattice constant to AISe.[19] However, the direct synthesis of AISe and AIS do not offer the same degree of control as Cd or Pb based binary QDs and AISe/AIS QDs have not been grown by heteroepitaxial overgrowth to date, probably due to the challenge of simultaneously controlling the reactivity of multiple precursors.

Here, we developed colloidal NIR-active AISe/AIS thick-shell QDs for solar energy conversion. To control the QDs growth, we employed the sequential cation exchange method,[20] with Cd-based QDs as templates. Unlike the irregular shape and broad size distribution of typical directly synthesized AIS or AISe QDs,[21] the size, core/shell interface and shape of QDs can be finely adjusted by tuning the initial templates, as observed from transmission electron microscopy (TEM) imaging. The absorption edge of QDs was successfully extended to the NIR window by cation exchange, making these materials suitable for solar light harvesting. To decrease the possible core–shell interface defects and regulate the charge transfer dynamics, we tuned the shell composition from AIS to AISeS by modulating the Se:S ratio during the monolayer-shell growth of template QDs.[12,14,20e,22] With the incorporation of AISeS alloy shell, the electron and hole wavefunction exhibits increasing leakage from core to shell region, which is consistent with the shorter PL lifetime of AISe/AISeS/AIS QDs (≈137 ns) than AISe/AIS QDs (≈172 ns), indicating the gradient shell should favor the electron/hole transfer process. As a proof of concept, we employed AISe, AISe/AIS and AISe/AISeS/AIS QDs for PEC system, where the saturated photocurrent density of AISe/AISeS/AIS QD-PEC is ≈3 and 1.5 times that of AIS and AISe/AIS under one-sun illumination, respectively. Due to the alleviated hole-induced self-oxidation, the AISe/AISeS/AIS QD-PEC also presented better stability than AISe/AIS. Our investigations illustrate a new route to synthesize eco-friendly NIR-active AISe/AIS ternary-core/ternary-shell QDs. This work also demonstrates that the interfacial design in core/shell QDs plays a key role in employing QDs for solar energy conversions, such as PEC H_2 generation and photovoltaic devices.

2. Results and Discussion

2.1. Synthesis and Structure of Thick-Shell QDs

The synthetic approach is schematically depicted at the top of **Figure 1**a. We started with the synthesis of CdSe QDs via a hot-injection method.[23] Subsequently, six monolayers of CdS shell were grown by the successive ionic layer adsorption and reaction (SILAR) method under N_2 flow to form CdSe/6CdS QDs (Figure S1, Supporting Information).[10e,24] To control the potential barrier and alleviate the lattice mismatch at the core–shell interface, we modulated the Se:S ratio during the growth of each $CdSe_xS_{1-x}$ (x = 0.9–0.1) shell layer with the same batch of CdSe core (Table S1, Supporting Information), forming CdSe/5$CdSe_xS_{1-x}$/CdS QDs (five monolayers of CdSeS and one monolayer of CdS).[14,22] Figure 1b,c displays transmission electron microscopy (TEM) images of Cd-based template QDs. With the same batch of CdSe QDs as core (radius of ≈1.7 nm, Figures S2 and S3, Supporting Information), both CdSe/6CdS and CdSe/5$CdSe_xS_{1-x}$/CdS QDs exhibit quasi-spherical shapes. The shell thickness of CdSe/5$CdSe_xS_{1-x}$/CdS was calculated to be 2.2 nm (Table S2, Supporting Information), which is slightly thicker than that of CdSe/6CdS (2.1 nm), probably due to the larger lattice space of CdSe compared with CdS.[25] The corresponding X-ray diffraction (XRD) patterns (Figure S1b, Supporting Information) illustrate that the CdSe QDs crystallize in the zinc blende (ZB) crystal structure (JCPDS No. 00-019-0191).[10c] After CdS shell growth, the diffraction pattern is dominated by the CdS wurtzite (WZ) crystal structure (JCPDS Card No. 01-077-2306), while the CdSe ZB is less visible, due to the large volume ratio of the CdS shell.[24a] In comparison, the XRD pattern of CdSe/5$CdSe_xS_{1-x}$/CdS QDs exhibits a mixed reflection between WZ CdS and WZ CdSe, which is consistent with selected area electron diffraction (SAED) patterns in Figure 1d, indicating the formation of alloyed CdSeS with WZ structure.

By mixing Cd-based QDs with a methanolic solution of $AgNO_3$ at room temperature, a rapid color change from yellow to brown was observed.[20a,d] The corresponding energy-dispersive X-ray spectroscopy (EDS) spectra confirmed the presence of Ag, Se and S, while Cd was barely detected (Figure S4, Supporting Information), suggesting that Cd was almost completely substituted by Ag. To replace Ag^+ with In^{3+}, we employed dodecanethiol (DDT) as Ag^+ extracting agent, which is a softer base than amines and can effectively bind to Ag^+ ions while preserving the QDs' integrity.[26] The corresponding EDS spectrum (Figure S4c, Supporting Information) and X-ray photoelectron spectroscopy (XPS) survey spectrum (Figure S5, Supporting Information) verified the presence of Se, Ag, In, and S, consistent with the chemical composition of (Ag,In)-based QDs. Inductively coupled plasma-optical emission spectrometry (ICP-OES) only observed ≈0.3% residual Cd after cation exchange (Table S3, Supporting

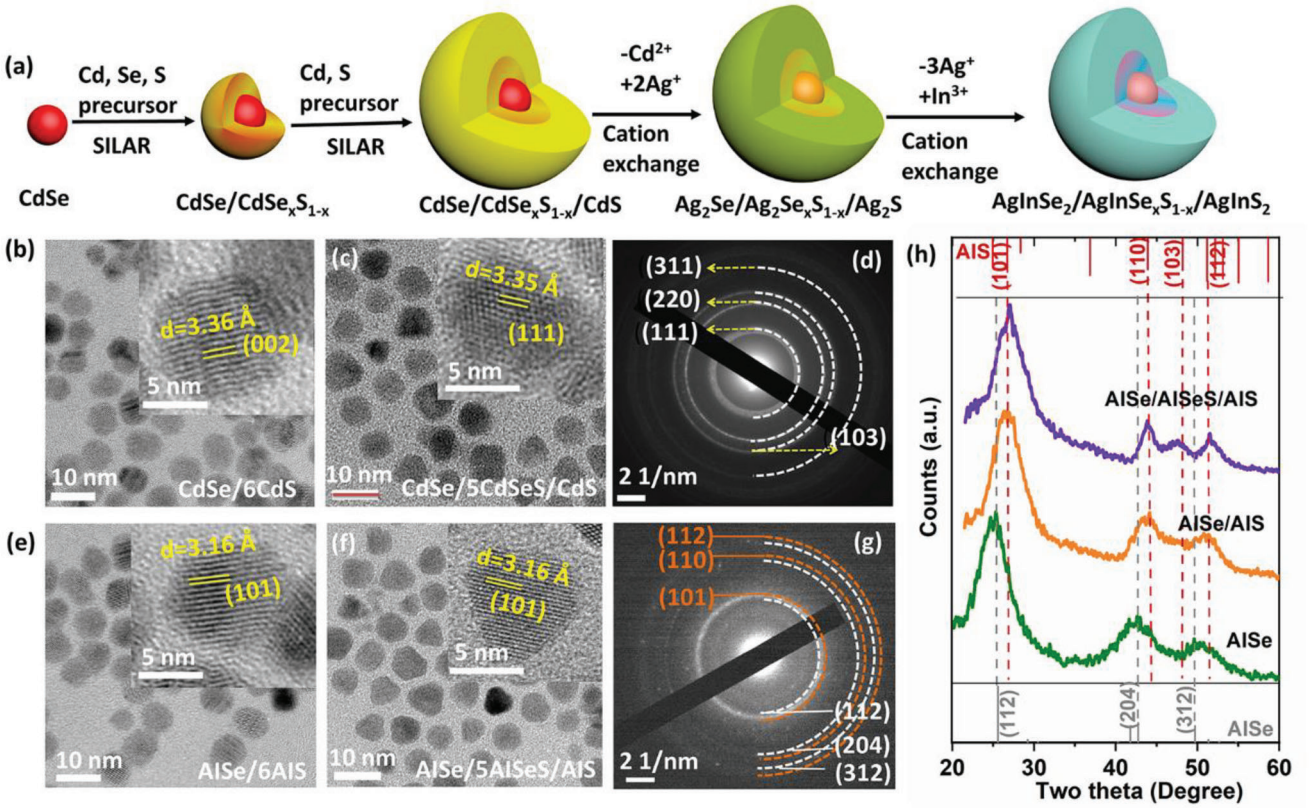

Figure 1. (a) Schematic illustration of sequential cation exchange reactions for the synthesis of AISe/AIS and AISe/AISeS/AIS QDs. Representative TEM images of b) CdSe/6CdS and c) CdSe/5CdSe$_x$S$_{1-x}$/CdS. d) SAED patterns of CdSe/5CdSe$_x$S$_{1-x}$/CdS QDs. Representative TEM images of e) AISe/AIS and f) AISe/AISeS/AIS QDs. g) SAED patterns of AISe/AISeS/AIS QDs. The inset high-resolution TEM images show the planes. h) X-ray powder diffraction (XRD) patterns of QDs after sequential cation exchange: AISe QDs (green curve), AISe/AIS QDs (orange curve), and AISe/AISeS/AIS QDs (violet curve). The Joint Committee on Powder Diffraction Standards (JCPDS) card files for AISe (JCPDS Card No. 00-035-1099) and AIS (JCPDS Card No. 01-089-5020).

Information), which can be considered as a full exchange of Cd. Based on XPS and ICP-OES, the Ag:In stoichiometry was found to be ≈1:1, indicating that the cation exchange reaction between Ag and In was a partial exchange that ended when a ternary composition was attained (Figure S6, Supporting Information). The incomplete exchange can be understood by considering the reorganization of the anionic sublattice. For example, In_2S_3 has an fcc stacking of S^{2-}, which is intrinsically different from the hcp anion sublattice of Ag_2S.[26a] The lattice and stoichiometric mismatch between Ag_2S and In_2S_3 inhibits complete exchange consequently.[26a]

Following the same cation exchange approach, (Ag,In)-based QDs including AISe, AISe/AIS, and AISe/AISeS/AIS were prepared. Unlike the irregular shapes after direct synthesis,[21] the Ag-based QDs exhibit quasi-spherical shapes after cation exchange (Figure 1e,f), with no noticeable change in shape (Figure 1b,c) and size (Figure S3, Supporting Information) in comparison to template QDs. The preservation of template morphology suggests this cation exchange method is effective to control the morphology of multinary QDs by rationally adjusting the initial QD templates. The HRTEM images of AISe QDs reveal a lattice spacing of ≈3.46 Å that can be indexed to the (112) plane of the cubic ZB phase of AISe (Figure S2, Supporting Information), which is consistent with the XRD patterns (JCPDS No. 00-035-1099) in Figure 1h. After AIS shell passivation, a lattice space of 3.16 Å was observed (Figure 1c), which can be indexed to the (101) planes of the hexagonal crystal structure of AIS (JCPDS No. 01-089-5020). An obvious plane overlap for AISe and AIS is present in the SAED patterns of AISe/AISeS/AIS (Figure 1e), which is consistent with the mixed XRD patterns of AISe and AIS for AISe/AISeS/AIS (Figure 1f), further confirming the formation of alloyed AgInSeS shell.

2.2. Optical Properties of QDs

As shown in **Figure 2**a, the absorption spectra of the template Cd-QDs span from the UV to the visible region (up to 650 nm). The first excitonic peak of CdSe QDs centered at 565 nm (Figure 2a) gives an estimation of QD diameter of 3.4 nm,[27] which is consistent with the average size observed from TEM images (Figure S3, Supporting Information). After adding CdS layers, the first excitonic peak redshifted to 592 nm, indicating a transition to the core/shell structure, rather than the alloyed structure.[10c,28] With the incorporation of the CdSe$_x$S$_{1-x}$ shell, the first-excitonic absorption peak further redshifted to 628 nm, as expected due to the narrower bandgap of CdSe (1.75 eV) compared to CdS (2.4 eV).[18,24b] After sequential cation exchange (Figure 2b), the

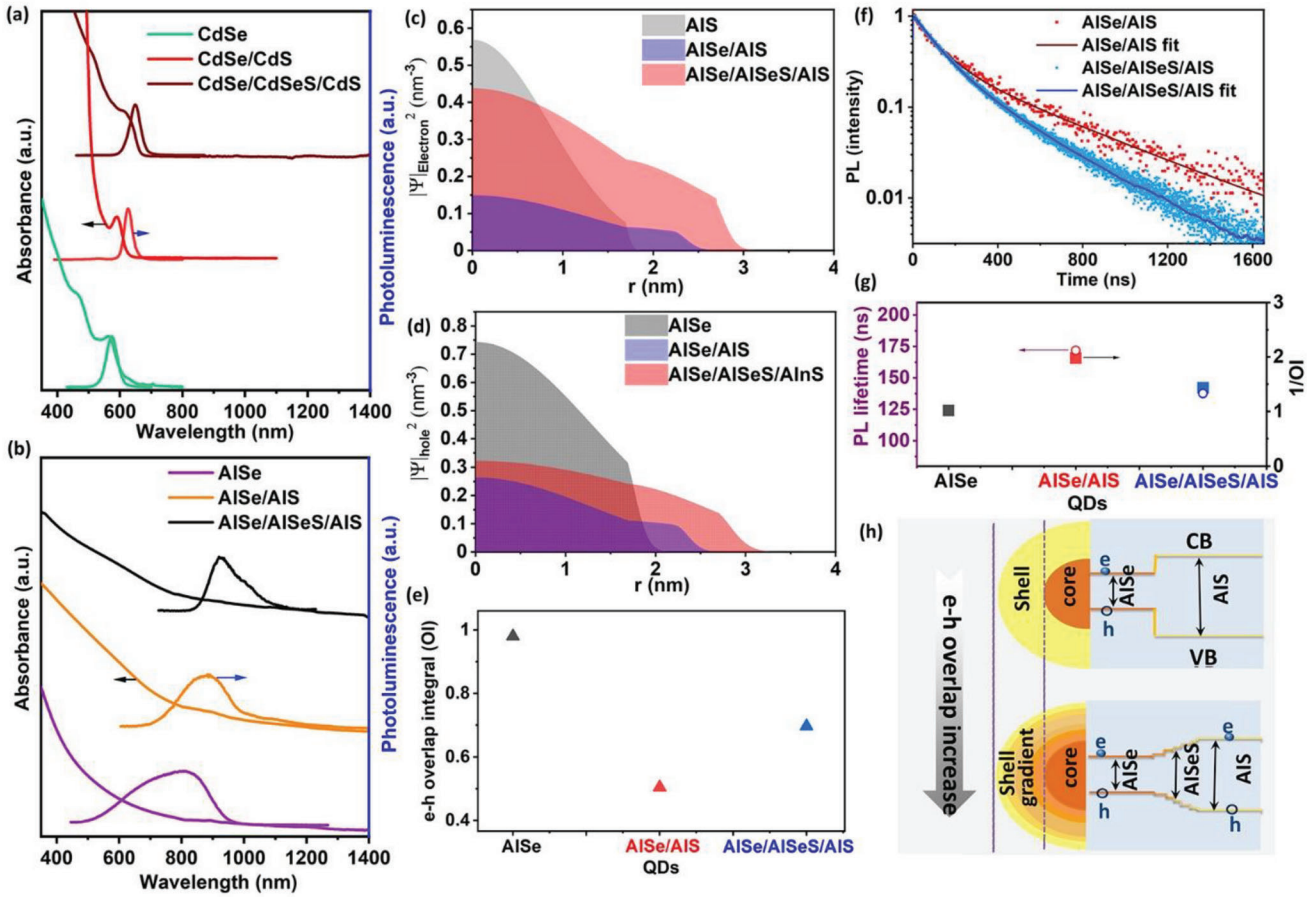

Figure 2. Absorption and PL spectra of a) CdSe (green curve), CdSe/6CdS (red curve), and CdSe/5CdSe$_x$S$_{1-x}$/CdS (brown curve), and b) AISe (purple curve), AISe/AIS (orange curve), and AISe/AISeS/AIS (black curve) QDs in toluene. The excitation wavelength is 444 nm. The norm squared of the wave function along a radial cut beginning at the center of the QDs, for c) 1 s electrons and d) 1 s holes. e) The overlap integral between the electrons and holes of AISe, AISe/AIS, and AISe/AISeS/AIS with $R = 1.7$ nm and $H_{shell} = 2.2$ nm, compared with the experimental lifetimes. f) Transient PL spectra of AISe/AIS and AISe/AISeS/AIS QDs in toluene. g) Comparison of the 1/OI with the experimental lifetime. h) Possible band structures of core/shell and core/gradient shell/shell QDs.

absorption spectra extend to the NIR region, while the first-excitonic peaks from Cd-QDs have disappeared. The excitonic peaks of QDs are poorly resolved, which is a typical feature of ternary I-III-VI QDs.[29] Simultaneously, the PL peaks of all QDs shifted from 570–640 to 820–870 nm, respectively (Figure 2b), suggesting the formation of (Ag, In)-based QDs. The significant extension of the absorption spectra after cation exchange also highlights the photons harvesting ability of (Ag,In)-based QDs, in the context of solar energy conversion.

By changing the shell from AIS to AISeS, the PL peak position of (Ag, In)-QDs gradually redshifted from 856 to 872 nm (Figure 2b). However, this redshift may not be due to size effects, because the size and morphology of the core are almost preserved during shell growth. To gain more insight into the nature of this redshift, we calculated the electron/hole wave functions [ψ_e(r) and ψ_h(r)] of (Ag, In)-based QDs based on the first-principles wave function file (WAVECAR) combined with the Schrödinger equation of finite deep potential (details are in the Supporting Information). The calculation yielded $\psi_e{}^2$(r) and $\psi_h{}^2$(r) as a function of QD radius, which is shown in Figure 2c,d, respectively. Along a line beginning at the center of the QDs, both electrons and holes of AISe/AISeS/AIS show an increased leakage into the shell region compared to that of AISe/AIS QDs. The overlap integral (OI) of the photoexcited carriers was calculated to semiquantitatively illustrate the carrier leakage from core to shell[30]

$$OI = \left| \int \psi_e(r)\, \psi_e(h)\, d^3r \right|^2 \quad (1)$$

The OI of AISe/AISeS/AIS and AISe/AIS are smaller compared to AISe (Figure 2e), indicating that the shell confines the electrons and holes in the core region. Therefore, the electron/hole transfer from the core to the charge acceptor may be hindered by the core-shell interfacial potential. The OI increases moving from AISe/AIS to AISe/AISeS/AIS, indicating that the AISe/AISe/AIS QDs present a larger e-h overlap in the shell region. The exciton delocalization from the core into the shell explains the PL redshift,[10e,24] which also agrees with the PL redshift of template Cd-QDs (from 612 nm of CdSe/CdS to 649 nm of CdSe/CdSeS/CdS, Figure 2a). This model assumes that the radiative charge recombination occurs between the

CB minimum and VB maximum and there is no impurity in the core. Therefore, with increasing electron–hole overlap, the oscillator strength of excitonic recombination will increase, decreasing the exciton radiative lifetimes. In this context, transient fluorescence spectroscopy was applied to investigate the exciton dynamics of (Ag,In)-based QDs (Figure 2f).[10e,12] The detailed fitting parameters and results are reported in Table S4 (Supporting Information). The AISe/AIS QDs present an average PL lifetime of ≈172 ns, which is much longer than its template CdSe/CdS QDs (≈50 ns, Figure S7, Supporting Information). This long lifetime is one of PL characteristic features of I-III-VI ternary QDs due to the interpretation of defect-state-based energy transitions.[31] When the gradient shell was added at the core-shell interface (AISe/AISeS/AIS), the average PL lifetime drops to be ≈137 ns (Figure 2f), which agrees well with the decreased 1/OI in Figure 2g. This observation demonstrates that the carrier distribution can be modulated by engineering the interfacial layers between AISe and AIS. In particular, in (Ag,In)-based QDs with shell thickness greater than 1.5 nm, the probability of finding the electrons and holes in the shell of the AISe/AISeS/AIS QDs is significantly higher than AISe/AIS (Figure S10, Supporting Information). The alloyed AISeS can provide a favorable stepwise band alignment to reduce the energy barrier for charge transfer, giving AISe/AISeS/AIS thick-shell QDs an advantage over AISe/AIS in terms of solar-energy conversion.

2.3. PEC Performance

Proof-of-concept PEC investigations were performed with AISe, AISe/AIS, and AISe/AISeS/AIS QDs as photosensitizers for photoanodes. All the fabricated PEC devices were measured under identical preparation and measurement conditions. By using the electrophoretic deposition (EPD) approach,[32] as-synthesized QDs were deposited into mesoporous TiO_2 films. The cross-sectional SEM image of the QD-based photoanode (**Figure 3**a) indicates that the thickness of the mesoporous TiO_2 film was around 14 μm. The 2D EDS map (Figure 3b–e) and the TEM images of QDs/TiO_2 (Figure S11, Supporting Information) illustrate that the QDs were homogeneously distributed in the TiO_2 film without noticeable agglomeration, suggesting the successful QDs deposition by EPD process. The chemical states and composition of the AISe/AISeS/AIS QDs after EPD were verified by high-resolution XPS. The Ag 3d, In 3d, Se 2p, and S 2p spectra (Figure 3f–i) indicate the valence state of Ag^+,[33] In^{3+},[30,34] Se^{2-},[35] and S^{2-},[36] respectively. After EPD, no significant variation in XPS spectral shift was detected, indicating that no obvious oxidation defects or surface traps were formed on QDs after deposition.[32]

PEC analysis was carried out using a three-electrode configuration,[8,12] where a platinum (Pt) foil works as a counter electrode and an Ag/AgCl saturated with KCl was used as the reference electrode. A mixture of aqueous 0.25 M Na_2S and 0.35 M Na_2SO_3 (pH ≈ 13) was used as an electrolyte and a sacrificial hole scavenger which prevents the photocorrosion of QDs.[13] To suppress the surface defects and reduce the charge recombination between TiO_2 and the electrolyte,[13,37] ZnS passivation layers were then grown on the photoanode by SILAR (two cycles).[12,13] Under simulated solar illumination (AM 1.5 G, 100 mW cm^{-2}), the photogenerated excitons in QDs dissociate at two interfaces: QDs/TiO_2 and QDs/electrolyte (**Figure 4**a). Driven by favorable band offset between QDs and TiO_2, electrons will leak from the core to the shell region followed by injection into the CB of TiO_2. Subsequently, the electrons are collected by FTO and reach the Pt counter electrode through the external circuit, reducing water into H_2.[8] Meanwhile, the dissociated holes of QDs can be captured by the hole scavenger (S^{2-}) in the electrolyte.

The photocurrent density under illumination gradually increased with the voltage until a saturated photocurrent density was obtained. Compared to the bare TiO_2 photoanode (Figure S12, Supporting Information), the TiO_2|AISe photoanode presented a 1.6-fold enhancement in saturated photocurrent density (Figure 4b, ≈0.38 mA cm^{-2} at 0.1 V vs RHE), which is mainly attributed to the improved light absorption from QDs.[13] After AIS shell passivation, the saturated photocurrent densities of AISe/AIS QD-photoanodes presented a further twofold enhancement compared to TiO_2|AISe (Figure 4c). With the introduction of the gradient layer, the saturated photocurrent densities of AISe/AISeS/AIS QD-photoanodes can be further improved to ≈3-fold compared to TiO_2|AISe (Figure 4d). This observation can be understood by considering the possible charge dynamics at the interfaces. In the TiO_2|AISe, the injection of AISe electrons into TiO_2 contributes to the photocurrent, while the severe charge recombination arising from surface traps of AISe may yield a relatively low current density.[10e,13] In the core/shell structure, the AIS shell can decrease the trap states and suppress electron–hole recombination at the TiO_2|QDs interface, increasing the current density. However, the holes need to overcome the original high energy barrier of the shell to react with the electrolyte, increasing the possibility of charge recombination at the QDs|electrolyte. In comparison, the AISeS gradient layer can serve as a ladder for electrons and holes to overcome the original energy barrier, facilitating the charge transfer at TiO_2/QDs and QDs|electrolyte simultaneously. Besides, the defects created by the lattice mismatch between the core and shell can be reduced,[14,22] consequently yielding a higher photocurrent density.

To further verify the role of the gradient shell in QDs, the stability of the PEC devices (saturated photocurrent density versus time) was investigated under one-sun illumination, with 0.2 V versus RHE potential applied (Figure 4e). The photocurrent densities of the TiO_2|AISe QD-PEC cells gradually decrease during illumination, with a drop equal to 50% of the original value after ≈400 s. With the presence of the thick shell, the photocurrent density of TiO_2|AISe/AIS and TiO_2|AISe/AISeS/AIS QD-PEC dropped to 50% of the original value after a longer duration of ≈2660 and ≈3800 s, respectively, proving the effective protecting role of the shell. The lower PEC stability of AISe/AIS compared to AISe/AISe/AIS could be due to the hole-accumulation-induced self-oxidative decomposition of QDs,[12] as a consequence of the presence of a thick shell as the charge-blocking layer, which is consistent with the charge transfer dynamics discussed above. The H_2 generation rate was estimated by using Faraday's law (calculation details are reported in the Supporting Information), with a faradic efficiency of ≈80% employed according to the reference curve of CdSe/CdS QDs.[10e,20e] By integrating the current density, the H_2 generation rate of TiO_2|AISe/AISeS/AIS QD-PEC reaches around 1.4 times that of TiO_2|AISe/AIS|ZnS (Figure S12,

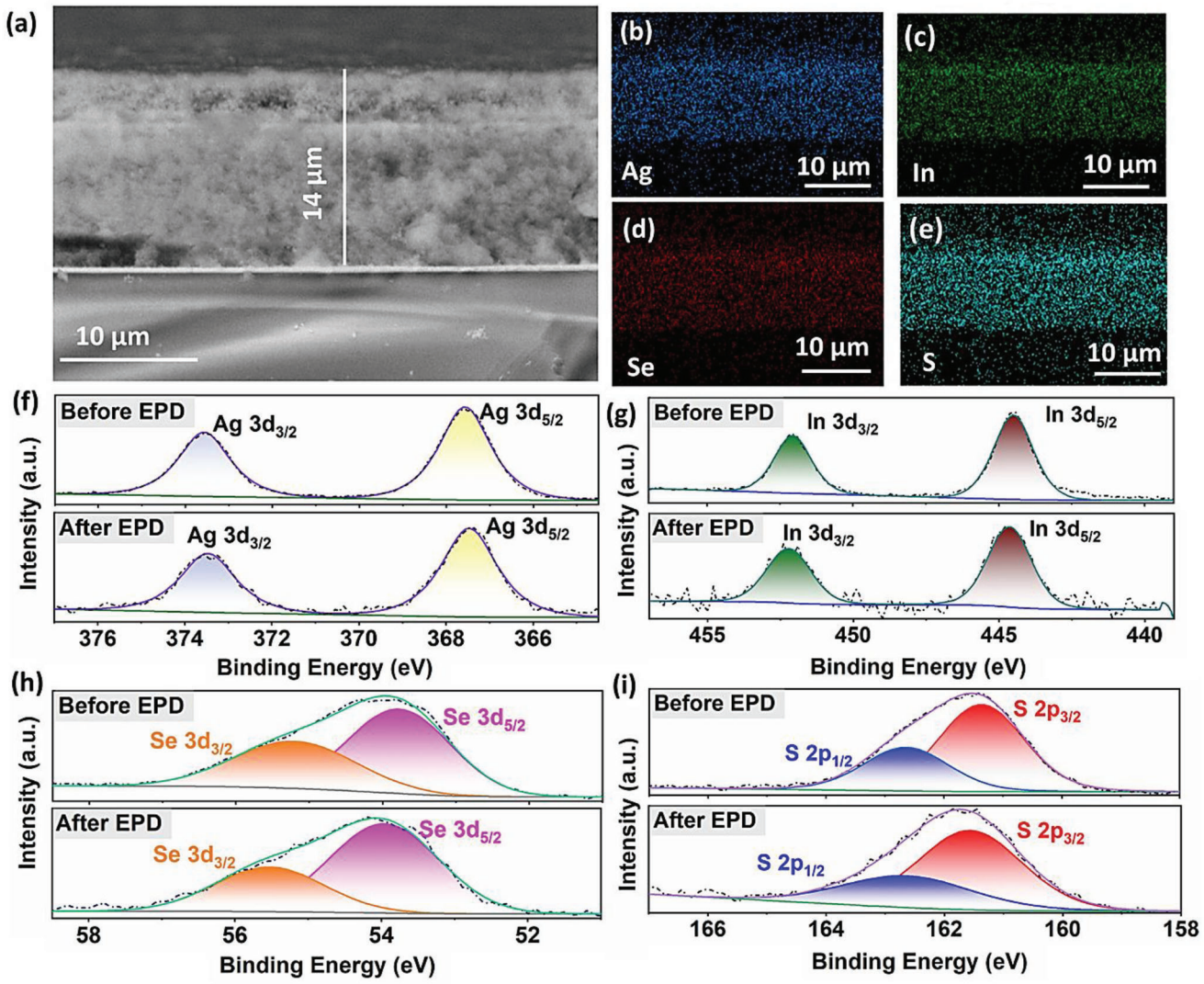

Figure 3. a) Typical cross-sectional SEM image of Glass|FTO|compact TiO_2|meseporous TiO_2-QDs|AISe/AISeS/AIS QDs photoanode architecture, and the corresponding 2D EDS mapping of the chemical composition including the essential elements: b) Ag, c) In, d) Se, and e) S. High-resolution XPS spectra of AISe/AISeS/AIS QDs: f) Ag, g) In, h) Se, and i) S before and after EPD.

Supporting Information), which can be assigned to the beneficial effect of AISeS layer.

3. Conclusions

In summary, eco-friendly thick-shell (Ag, In)-based core/shell QDs were successfully synthesized via a sequential cation exchange method. Different from the irregular morphology of direct synthesis, the sizes, shapes and structures of (Ag, In)-based QDs can be rationally controlled by regulating the Cd-based template QDs. Full cation replacement of Cd with Ag and In extended the light absorption of QDs to the NIR region, improving solar light harvesting. In particular, based on our exciton dynamic investigation and theoretical calculation, the introduction of a gradient AISeS interfacial shell could potentially facilitate charge transfer from core to charge acceptors, which may improve solar energy conversion. As a proof of concept, we employed these (Ag, In)-based QDs for the PEC system, where the AISe/AISeS/AIS QD-PEC exhibited higher saturated photocurrent density and better stability in comparison to AISe and AISe/AIS QDs. The better PEC performances of AISe/AISeS/AIS QD-PEC can be ascribed to the energy gradient in the electronic band between the core and the outer shell, which can balance passivation and the charge transfer from core to shell. The future progress of the above system could focus on the optimization of charge transport by suitable engineering of surface ligands, such as partially or fully exchanging the initial long-chain ligands with shorter-chain surfactants. This investigation not only opens new routes toward size-, shape-, and composition-controlled ternary $AgInX_2$ (X = Se, Te, S) nanocrystals but also proposes the AISe/AISeS/AIS QDs as promising candidates for optoelectronic devices that require absorption/PL spectrum spanning across the UV–visible–NIR regions (such as fluorescent biosensors, solar cells, and LSCs).

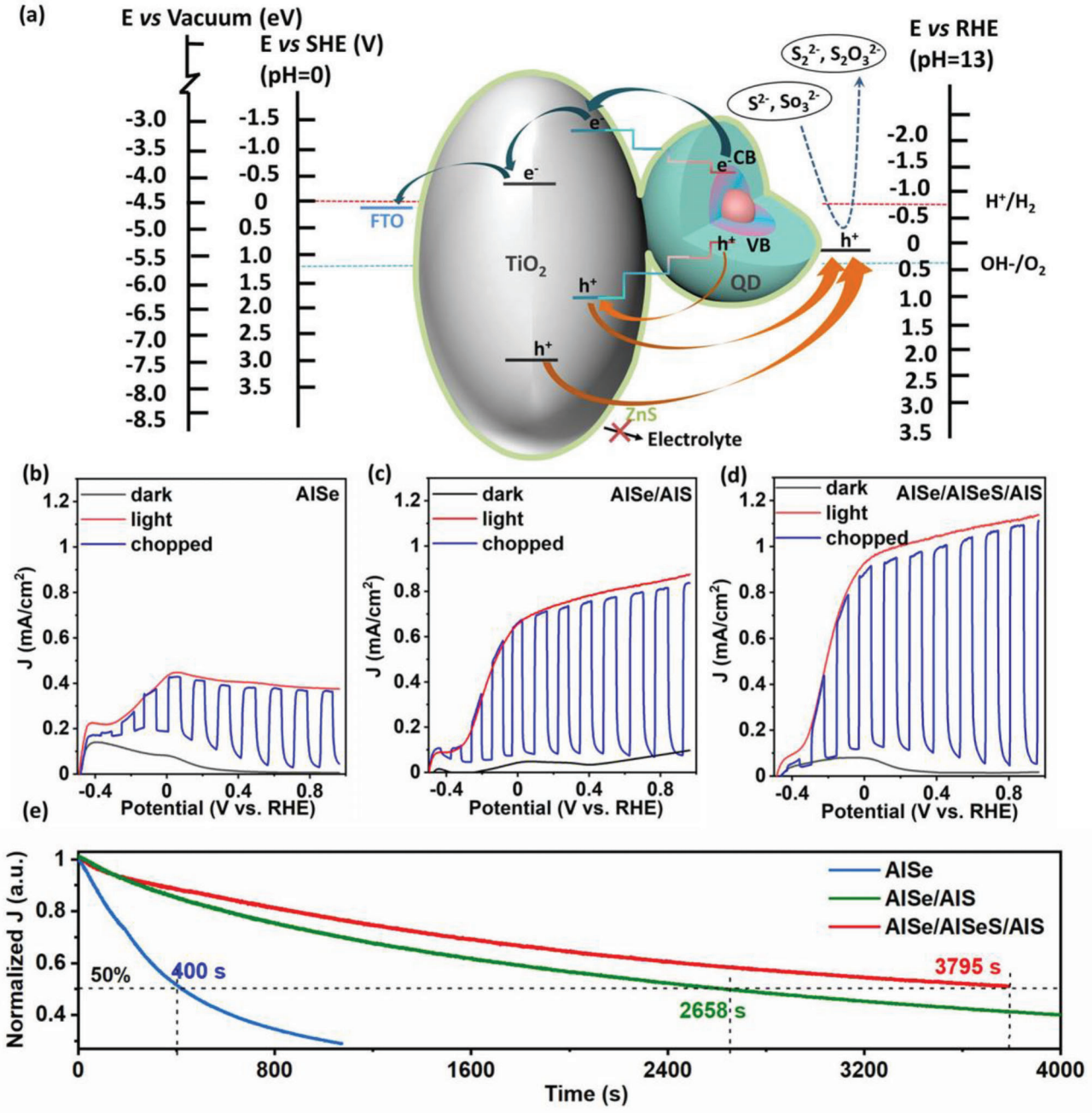

Figure 4. The approximate band alignment and schematic diagram of AlSe/AlSeS/AlS QDs sensitized TiO_2 photoanodes. The arrows indicate the electron (blue) and hole (orange) transfer process. Photocurrent density–potential dependence of b) FTO|TiO_2|AlSe QDs|ZnS, c) FTO|TiO_2|AlSe/AlS QDs|ZnS, and d) FTO|TiO_2|AlSe/AlSeS/AlS QDs|ZnS in the dark (black curve), under chopped (blue curve) and continuous (red curve) one-sun illumination (AM 1.5 G, 100 mW cm^{-2}). e) *J–t* plots of representative photoanodes under one-sun illumination at 0.2 V versus Ag/AgCl.

4. Experimental Section

Synthesis of Cd-Based Template QDs: The CdSe core QDs were synthesized with the hot injection approach.[23] Deposition of CdS layers on CdSe was realized using SILAR.[10e,22] 0.2 M [Cd(oleate)$_2$] dispersed in 1-octadecene (ODE) was dropwise injected into CdSe QDs (≈2 × 10^{-7} mol) solution via syringe and the reaction proceeded for 1.5 h at 240 °C. Subsequently, 0.2 M solution of elemental sulfur in ODE with the same volume was dropwise injected and annealed for 10 min. The quantity of precursors for growing each monolayer of the shell was calculated and S/Cd(oleate)$_2$ injection volumes for shell deposition cycles are summarized as follows: 0.31, 0.43, 0.58, 0.75, 0.94, and 1.15 mL. For the growth of the alloyed shell QDs, a mixture of S/Se (different molar ratios of S:Se with a total concentration of 0.2 M) was used.

Cation Exchange Procedure: Typically, for Ag^+ cation exchange,[20d] $AgNO_3$ (0.4 mmol) mixed with methanol (4 mL) and toluene (4 mL) was added to Cd-based QDs (≈2 × 10^{-8} mol in toluene) in a flask. The reaction proceeded for 10 min at room temperature with vigorous stirring.

Subsequently, the as-synthesized Ag-based QDs were centrifuged, washed by precipitation/redispersion with methanol and toluene, and redispersed in 5 mL of toluene.

For In^{3+} cation exchange,[26b] the indium stock solution was presynthesized by heating the mixture of $In(OAc)_3$ (0.1 mmol), oleylamine (OA) (2 mL), and 1-dodecanethiol (DDT) (1 mL) to 170 °C to disperse the $In(OAc)_3$ well in the solution. The Ag-based QDs were degassed by N_2 to remove toluene and then dispersed into 5 mL of ODE and 2 mL of DDT. The reaction mixture was then heated to 100 °C under N_2 flow. Subsequently, the indium stock solution was dropwise injected into the solution when the temperature was stable at 100 °C. The mixture was maintained at 100 °C for 120 min and then cooled down to room temperature. The as-synthesized (Ag,In)-based QDs were precipitated with ethanol, centrifuged to eliminate unreacted precursors, and redispersed in toluene.

Preparation of Photoanode: A thin and compact TiO_2 blocking layer was obtained by spin-coating Ti-Nanoxide BL/SC on fluorine-doped tin oxide (FTO) glass substrates, annealing in a furnace at 500 °C for 60 min. Subsequently, a commercial TiO_2 paste (18NR-AO) was deposited on top of the compact TiO_2 layer by tape casting to obtain the mesoporous TiO_2 films after annealing. The QDs sensitization of TiO_2 photoanode was realized by EPD.[32] Successively, two cycles of the ZnS capping layer were then grown using the in situ SILAR method.[10e,13]

Characterization: TEM images of QDs and TiO_2/QDs were acquired by using a JEOL 2100F TEM. The cross-sectional SEM and EDS chemical composition mapping of the FTO/TiO_2/QDs photoanode were performed using a JSM-6900F microscope. The XRD pattern of purified QDs film deposited on a glass substrate was performed using a Panalytical X-Pert PRO MRD with Cu Kα radiation source ($\lambda = 0.15418$ nm). UV–visible–NIR absorption spectra were measured using a Cary 5000 UV-visible-NIR spectrophotometer. PL spectra and PL lifetime of the QDs in solution were acquired via a Fluorolog-3 system equipped with a DeltaHub controller (Horiba Jobin Yvon). ICP-OES was performed using an Agilent 5100 ICP-OES system. XPS was performed using a VG Escalab 220i-XL equipped with a hemispherical analyzer, applying a Twin Anode X-Ray Source. The C 1s peak (calibrated to a binding energy = 284.6 eV) was used as an intrinsic reference to rule out charging effects. The fine structure of the photoelectron lines was treated using Casa XPS software (2.3.15 Version). All electrochemical measurements were performed by using a Gamry 1000E electrochemical workstation with a sweep rate of 20 mV s^{-1}. A traditional three-electrode system was used to evaluate the PEC performance of the QDs-sensitized photoanode, with a platinum sheet as a counter electrode and an Ag/AgCl with saturated KCl as a reference electrode.[10e,13] The electrolyte (pH = 13) was composed of 300 mL water 0.25 M $Na_2S{\cdot}9\,H_2O$ and 0.35 M Na_2SO_3. A Compact Solar Simulator AAA (Sciencetech SLB-300A) was used to provide simulated sunlight.

Theoretical Calculations: In this work, the first-principles calculation steps were completed through structural optimization, static self-consistent field (SCF), the density of state, energy band calculation, and charge calculation. All calculation steps were completed by VASP-6.1.0,[38] combined with the PBE functional[39] under the generalized gradient approximation (GGA)[40] in the frame of density functional theory (DFT) with Hubbard U model for strong correlation elements and D3 dispersion correction,[41] combined with the projector augmented wave (PAW),[42] and the plane wave cut-off energy is 500 eV. Among them, the 9*9*1 and 11*11*11 K mesh for surface/interface and bulk model. The wave function of QDs was realized by the first-principles wave function file (WAVECAR) combined with the Schrödinger equation of finite deep potential.

Supporting Information

Supporting Information is available from the Wiley Online Library or from the author.

Acknowledgements

F.R. and D.F.P. acknowledge funding from the Natural Science and Engineering Research Council of Canada (NSERC) and the Canada Foundation for Innovation (CFI), and the Fonds de recherche du Québec – Nature et technologies (FRQNT). F.R. is also grateful to the Canada Research Chairs program for partial salary support. L.J. acknowledges FRQNT for the financial support. L.J. also acknowledges the financial support from the Postdoctoral Research Foundation of China (Grant No. 2020M673173) and the National Natural Science Foundation of China (Grant No. 22005044). D.B. acknowledges FRQNT Postdoctoral Fellowship (No. 316170) for the financial support. G.S.S acknowledges DAL-AC for the financial support. X.T. acknowledges National Key Research and Development Program of China (No. 2019YFE0121600).

Conflict of Interest

The authors declare no conflict of interest.

Data Availability Statement

The data that support the findings of this study are available from the corresponding author upon reasonable request.

Keywords

cation exchange, core–shell structures, eco-friendly quantum dots, photoelectrochemistry, quantum dots

Received: February 1, 2023
Revised: March 14, 2023
Published online: April 19, 2023

[1] N. S. Lewis, *Science* **2007**, *315*, 798.
[2] a) O. K. Varghese, M. Paulose, C. A. Grimes, *Nat. Nanotechnol.* **2009**, *4*, 592; b) R. Nechache, C. Harnagea, S. Li, L. Cardenas, W. Huang, J. Chakrabartty, F. Rosei, *Nat. Photonics* **2015**, *9*, 61; c) R. Lin, J. Xu, M. Wei, Y. Wang, Z. Qin, Z. Liu, J. Wu, K. Xiao, B. Chen, S. M. Park, G. Chen, H. R. Atapattu, K. R. Graham, J. Xu, J. Zhu, L. Li, C. Zhang, E. H. Sargent, H. Tan, *Nature* **2022**, *603*, 73; d) J. Xu, O. Voznyy, M. Liu, A. R. Kirmani, G. Walters, R. Munir, M. Abdelsamie, A. H. Proppe, A. Sarkar, F. P. García de Arquer, M. Wei, B. Sun, M. Liu, O. Ouellette, R. Quintero-Bermudez, J. Li, J. Fan, L. Quan, P. Todorovic, H. Tan, S. Hoogland, S. O. Kelley, M. Stefik, A. Amassian, E. H. Sargent, *Nat. Nanotechnol.* **2018**, *13*, 456.
[3] A. P. Alivisatos, *Science* **1996**, *271*, 933.
[4] a) Y. Yan, R. W. Crisp, J. Gu, B. D. Chernomordik, G. F. Pach, A. R. Marshall, J. A. Turner, M. C. Beard, *Nat. Energy* **2017**, *2*, 17052; b) V. I. Klimov, *Annu. Rev. Phys. Chem.* **2007**, *58*, 635; c) J. R. Caram, S. N. Bertram, H. Utzat, W. R. Hess, J. A. Carr, T. S. Bischof, A. P. Beyler, M. W. Wilson, M. G. Bawendi, *Nano Lett.* **2016**, *16*, 6070.
[5] a) F. P. García de Arquer, D. V. Talapin, V. I. Klimov, Y. Arakawa, M. Bayer, E. H. Sargent, *Science* **2021**, *373*, eaaz8541; b) Z. Pan, H. Rao, I. Mora-Seró, J. Bisquert, X. Zhong, *Chem. Soc. Rev.* **2018**, *47*, 7659.
[6] M. Kim, J. Jeong, H. Lu, T. K. Lee, F. T. Eickemeyer, Y. Liu, I. W. Choi, S. J. Choi, Y. Jo, H.-B. Kim, S.-I. Mo, Y.-K. Kim, H. Lee, N. G. An, S. Cho, W. R. Tress, S. M. Zakeeruddin, A. Hagfeldt, J. Y. Kim, M. Grätzel, D. S. Kim, *Science* **2022**, *375*, 302.
[7] Y. Zhou, H. Zhao, D. Ma, F. Rosei, *Chem. Soc. Rev.* **2018**, *47*, 5866.
[8] L. Jin, H. Zhao, Z. M. Wang, F. Rosei, *Adv. Energy Mater.* **2021**, *11*, 2003233.
[9] M. Graetzel, R. A. Janssen, D. B. Mitzi, E. H. Sargent, *Nature* **2012**, *488*, 304.
[10] a) R. Ghosh Chaudhuri, S. Paria, *Chem. Rev.* **2012**, *112*, 2373; b) B. Mahler, P. Spinicelli, S. Buil, X. Quelin, J.-P. Hermier, B. Dubertret,

Nat. Mater. **2008**, *7*, 659; c) Y. Chen, J. Vela, H. Htoon, J. L. Casson, D. J. Werder, D. A. Bussian, V. I. Klimov, J. A. Hollingsworth, *J. Am. Chem. Soc.* **2008**, *130*, 5026; d) J. J. Li, Y. A. Wang, W. Guo, J. C. Keay, T. D. Mishima, M. B. Johnson, X. Peng, *J. Am. Chem. Soc.* **2003**, *125*, 12567; e) R. Adhikari, L. Jin, F. Navarro-Pardo, D. Benetti, B. AlOtaibi, S. Vanka, H. Zhao, Z. Mi, A. Vomiero, F. Rosei, *Nano Energy* **2016**, *27*, 265.

[11] a) J. Van Embden, J. Jasieniak, P. Mulvaney, *J. Am. Chem. Soc.* **2009**, *131*, 14299; b) F. Purcell-Milton, A. K. Visheratina, V. A. Kuznetsova, A. Ryan, A. O. Orlova, Y. K. Gun'ko, *ACS Nano* **2017**, *11*, 9207.

[12] L. Jin, G. Sirigu, X. Tong, A. Camellini, A. Parisini, G. Nicotra, C. Spinella, H. Zhao, S. Sun, V. Morandi, M. Zavelani-Rossi, F. Rosei, A. Vomiero, *Nano Energy* **2016**, *30*, 531.

[13] L. Jin, B. AlOtaibi, D. Benetti, S. Li, H. Zhao, Z. Mi, A. Vomiero, F. Rosei, *Adv. Sci.* **2016**, *3*, 1500345.

[14] G. S. Selopal, H. Zhao, G. Liu, H. Zhang, X. Tong, K. Wang, J. Tang, X. Sun, S. Sun, F. Vidal, *Nano Energy* **2019**, *55*, 377.

[15] P.-Y. Hsieh, T. Kameyama, T. Takiyama, K. Masuoka, T. Yamamoto, Y.-J. Hsu, T. Torimoto, *J. Mater. Chem. A* **2020**, *8*, 13142.

[16] I. Tsuji, H. Kato, A. Kudo, *Angew. Chem.* **2005**, *117*, 3631.

[17] Z. Liu, X. Yang, Z. Wang, H. Qi, L. Ji, X. Li, C. Ma, Z. Deng, J. Deng, *Mater. Lett.* **2015**, *161*, 442.

[18] S. Lade, M. Uplane, C. Lokhande, *Mater. Chem. Phys.* **2001**, *68*, 36.

[19] a) K.-W. Cheng, S.-C. Wang, *Mater. Chem. Phys.* **2009**, *115*, 14; b) G. Masse, E. Redjai, *J. Appl. Phys.* **1986**, *59*, 1544.

[20] a) D. H. Son, S. M. Hughes, Y. Yin, A. P. Alivisatos, *Science* **2004**, *306*, 1009; b) W. van der Stam, E. Bladt, F. T. Rabouw, S. Bals, C. de Mello Donega, *ACS Nano* **2015**, *9*, 11430; c) X. Tong, X. T. Kong, Y. Zhou, F. Navarro-Pardo, G. S. Selopal, S. Sun, A. O. Govorov, H. Zhao, Z. M. Wang, F. Rosei, *Adv. Energy Mater.* **2018**, *8*, 1701432; d) W. E. Benjamin, D. R. Veit, M. J. Perkins, E. Bain, K. Scharnhorst, S. McDowall, D. L. Patrick, J. D. Gilbertson, *Chem. Mater.* **2014**, *26*, 1291; e) F. Li, M. Zhang, D. Benetti, L. Shi, L. V. Besteiro, H. Zhang, J. Liu, G. S. Selopal, S. Sun, Z. Wang, *Appl. Catal., B* **2021**, *280*, 119402.

[21] a) W. Chen, J. Li, P. Liu, H. Liu, J. Xia, S. Li, D. Wang, D. Wu, W. Lu, X. W. Sun, *Sol. RRL* **2017**, *1*, 1700041; b) Z. Long, X. Tong, R. Wang, A. I. Channa, X. Li, Y. You, L. Xia, M. Cai, H. Zhao, Z. M. Wang, *ChemSusChem* **2022**, *15*, 202200346.

[22] K. Wang, X. Tong, Y. Zhou, H. Zhang, F. Navarro-Pardo, G. S. Selopal, G. Liu, J. Tang, Y. Wang, S. Sun, *J. Mater. Chem. A* **2019**, *7*, 14079.

[23] B. O. Dabbousi, J. Rodriguez-Viejo, F. V. Mikulec, J. R. Heine, H. Mattoussi, R. Ober, K. F. Jensen, M. G. Bawendi, *J. Phys. Chem. B* **1997**, *101*, 9463.

[24] a) Y. Ghosh, B. D. Mangum, J. L. Casson, D. J. Williams, H. Htoon, J. A. Hollingsworth, *J. Am. Chem. Soc.* **2012**, *134*, 9634; b) H. Zhao, D. Benetti, L. Jin, Y. Zhou, F. Rosei, A. Vomiero, *Small* **2016**, *12*, 5354.

[25] J. Zhang, Y. Tang, K. Lee, M. Ouyang, *Science* **2010**, *327*, 1634.

[26] a) H. Doh, S. Hwang, S. Kim, *Chem. Mater.* **2016**, *28*, 8123; b) B. Zeng, F. Chen, Z. Liu, Z. Guan, X. Li, F. Teng, A. Tang, *J. Mater. Chem. C* **2019**, *7*, 1307.

[27] W. W. Yu, L. Qu, W. Guo, X. Peng, *Chem. Mater.* **2003**, *15*, 2854.

[28] a) W. K. Bae, L. A. Padilha, Y.-S. Park, H. McDaniel, I. Robel, J. M. Pietryga, V. I. Klimov, *ACS Nano* **2013**, *7*, 3411; b) A. M. Dennis, B. D. Mangum, A. Piryatinski, Y.-S. Park, D. C. Hannah, J. L. Casson, D. J. Williams, R. D. Schaller, H. Htoon, J. A. Hollingsworth, *Nano Lett.* **2012**, *12*, 5545.

[29] a) H. McDaniel, N. Fuke, N. S. Makarov, J. M. Pietryga, V. I. Klimov, *Nat. Commun.* **2013**, *4*, 2887; b) R. Xie, M. Rutherford, X. Peng, *J. Am. Chem. Soc.* **2009**, *131*, 5691.

[30] F. Li, M. Zhang, D. Benetti, L. Shi, L. V. Besteiro, H. Zhang, J. Liu, G. S. Selopal, S. Sun, Z. Wang, *Appl. Catal., B* **2021**, *280*, 119402.

[31] O. Yarema, M. Yarema, D. Bozyigit, W. M. Lin, V. Wood, *ACS Nano* **2015**, *9*, 11134.

[32] L. Jin, H. Zhao, D. Ma, A. Vomiero, F. Rosei, *J. Mater. Chem. A* **2015**, *3*, 847;

[33] J. Hammond, S. Gaarenstroom, N. Winograd, *Anal. Chem.* **1975**, *47*, 2193.

[34] H. Zhong, Y. Zhou, M. Ye, Y. He, J. Ye, C. He, C. Yang, Y. Li, *Chem. Mater.* **2008**, *20*, 6434.

[35] J.-J. Wang, Y.-Q. Wang, F.-F. Cao, Y.-G. Guo, L.-J. Wan, *J. Am. Chem. Soc.* **2010**, *132*, 12218.

[36] A. Singh, H. Geaney, F. Laffir, K. M. Ryan, *J. Am. Chem. Soc.* **2012**, *134*, 2910.

[37] X. Tong, A. I. Channa, Y. You, P. Wei, X. Li, F. Lin, J. Wu, A. Vomiero, Z. M. Wang, *Nano Energy* **2020**, *76*, 105062.

[38] J. Hafner, *J. Comput. Chem.* **2008**, *29*, 2044.

[39] a) J. P. Perdew, K. Burke, M. Ernzerhof, *Phys. Rev. Lett.* **1996**, *77*, 3865; b) G. Kresse, D. Joubert, *Phys. Rev. B* **1999**, *59*, 1758.

[40] A. D. Becke, *J. Chem. Phys.* **1996**, *104*, 1040.

[41] S. Grimme, J. Antony, S. Ehrlich, H. Krieg, *J. Chem. Phys.* **2010**, *132*, 154104.

[42] P. E. Blöchl, *Phys. Rev. B* **1994**, *50*, 17953.

